PHYSICAL REVIEW B **93**, 140202(R) (2016)

Designing a fully compensated half-metallic ferrimagnet

Mario Žic,[1] Karsten Rode,[2] Naganivetha Thiyagarajah,[2] Yong-Chang Lau,[2] Davide Betto,[2] J. M. D. Coey,[2] Stefano Sanvito,[2] Kerry J. O'Shea,[3] Ciaran A. Ferguson,[3] Donald A. MacLaren,[3] and Thomas Archer[1,*]

[1]*CRANN and School of Physics, Trinity College Dublin, Dublin 2, Ireland*

[2]*CRANN, AMBER and School of Physics, Trinity College Dublin, Dublin 2, Ireland*

[3]*SUPA, School of Physics & Astronomy, University of Glasgow, Glasgow G12 8QQ, United Kingdom*

(Received 24 November 2015; published 1 April 2016)

Recent experimental work on Mn_2Ru_xGa demonstrates its potential as a compensated ferrimagnetic half metal (CFHM). Here we present a set of high-throughput *ab initio* density functional theory calculations and a detailed experimental characterization that enable us to correctly describe the nominal Mn_2Ru_xGa thin films, in particular, with regard to site disorder and defects. We then construct models that accurately capture all the key features of the Mn-Ru-Ga system, including magnetic compensation and the spin gap at the Fermi level. We find that electronic doping is necessary, which is achieved with a Mn/Ga ratio smaller than two. Our study shows how composition and substrate-induced biaxial strain can be combined to design a ferrimagnetic half metal with a compensation point close to room temperature.

DOI: 10.1103/PhysRevB.93.140202

Compensated ferrimagnetic half metals (CFHMs) have an ordered spin state with no net magnetic moment. As the material creates no stray magnetic field it should have low Gilbert damping, and offer numerous advantages compared to standard ferromagnetic metals. These include higher frequency operation, higher packing density, reduced device power requirement, and devices that are impervious to external magnetic fields. Although there is no net magnetic moment, the highly polarized spin state allows switching of the magnetization via spin-transfer torque. The class of CFHMs was first envisaged by van Leuken and de Groot [1] in 1995, but despite significant effort [2–7] the goal of a CFHM has proved elusive [8].

Recent experimental [9–11] and theoretical [12] efforts towards creating a CFHM have concentrated on the Heusler alloy system Mn_2Ru_xGa (MRG). Heusler alloys are made of four interlaced fcc lattices, which form a bcc-like structure. Mn_2RuGa has the full Heusler ($L2_1$) structure, with Mn occupying the 4*a* and 4*c* sites, Ru the 4*d*, and Ga the 4*b* sites [9]. Half-metallic Heuslers with the $L2_1$ structure are expected to follow a modified Slater-Pauling curve with the net magnetic moment m given by $m = N_v - 24$, where N_v is the number of valence electrons. For Mn_2RuGa, $N_v = 25$, resulting in a net moment of $+1\mu_B$. Mn_2Ga is expected to have a half-Heusler ($C1_b$) structure [13], with Mn on 4*a*,4*c* sites and Ga on 4*b* sites, thus leaving the 4*d* site empty. In half-metallic Heuslers with the $C1_b$ structure, the magnetic moment m is given by $m = N_v - 18$. For Mn_2Ga, $N_v = 17$ and hence $m = -1\mu_B$. The idea behind the Mn_2Ru_xGa system, as proposed by Kurt *et al.* [9], was that by changing the Ru content x, a material can be formed midway between Mn_2RuGa and Mn_2Ga that is half metallic yet presents no net magnetic moment.

Cubic Mn_2Ru_xGa was stabilized in thin film form by Kurt *et al.* [9], who showed that at $x \approx 0.5$ there is an ordered spin state with a critical temperature of approximately 550 K and a very small net magnetic moment. In the same work, point contact Andréev reflection (PCAR) spectroscopy showed a 54% spin polarization at the Fermi level. This is less than the 100% expected for an ideal half metal, but close to the values measured in other Heusler half metals in thin film form. Further evidence of half metallicity comes from the spontaneous Hall angle, more than an order of magnitude higher than that observed in the 3*d* transition metals. This and the linear variation of m with x provided strong indications that $Mn_2Ru_{0.5}Ga$, grown by Kurt *et al.* [9], was a CFHM.

However, despite the experimental evidence, the measurements do not match the theoretical understanding of Mn_2Ru_xGa provided by Galanakis *et al.* [12]. There are three main areas where disagreement between theory and experiment exists, namely, (1) the onset of half metallicity, (2) the cell volume, and (3) the dependence of M on x.

Half metallicity. Density functional theory (DFT) investigations of $Mn_2Ru_{0.5}Ga$ indicate that, although it may be possible to engineer a phase with zero magnetic moment, this will not be half metallic [3,5,12]. Our calculations and those of others [12,14] find that the spin gap in the density of states (DOS) of $Mn_2Ru_{0.5}Ga$ lies about 0.4 eV above the Fermi level E_F. In Fig. 1 we plot the calculated DOS and the corresponding resistivity, obtained by solving the Boltzmann equations in the relaxation time approximation. Although the DOS exhibits a large spin polarization, ≈60%, this is not reflected in that of the resistivity, which is only 30%. Since our transport calculations are expected to overestimate the spin polarization, the presence of the "pseudogap" [15] cannot justify the large experimentally observed spin polarization of the current.

Cell volume. X-ray diffraction (XRD) and transmission electron microscopy (TEM) demonstrate that the films grow epitaxially with the in-plane lattice parameter being dictated by the MgO substrate ($a_{MRG} = \sqrt{2}a_{MgO}$) for all film thicknesses grown, while the out-of-plane lattice parameter c depends strongly on the film thickness [10,16]. This results in cell volumes much larger than those predicted by DFT, and their variation with film thickness cannot be explained.

Magnetism. The measured magnetic moment as a function of Ru concentration is linear [9] for $0.3 \leqslant x \leqslant 0.7$ with slope $dM/dx = 2$, suggesting that there is a spin gap at the Fermi

*archert@tcd.ie; www.materials-mine.com

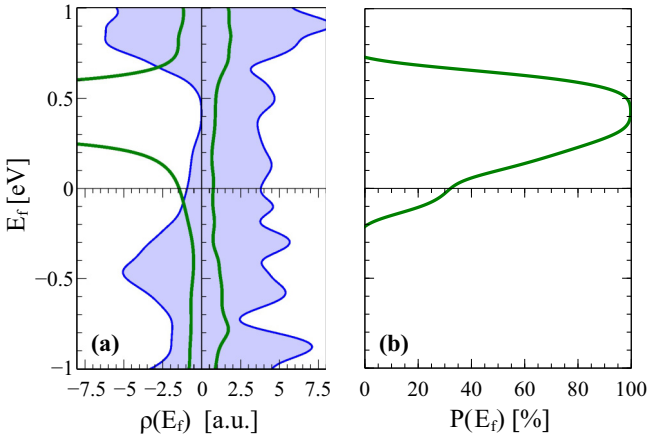

FIG. 1. (a) Spin resolved resistivity (green) and the corresponding density of states (DOS) (blue) calculated for the $Mn_2Ru_{0.5}Ga$. The data corresponding to the spin down channel are represented with negative values. (b) Calculated transport spin polarization.

level over an extended range of concentrations, in contradiction to the DFT results.

Here, we address and resolve the conflict between experiment and theory. By applying a high-throughput approach based on the VASP [17] implementation of DFT and the Perdew-Burke-Ernzerhof (PBE) [18] functional, we have calculated the properties of 1221 Heusler phases containing Mn, Ru, and Ga that present different stoichiometry, magnetic order, and site occupancy within the $L2_1$ and $C1_b$ symmetries [19]. Other symmetries were excluded from the search. For each configuration we compute the enthalpy of formation ΔH with respect to the lowest energy phase of each of the constituent elements, allowing us to compare the relative stability of the various configurations. Our results for the lowest energy structures are summarized in Table I.

TABLE I. Calculated enthalpies of formation ΔH for the most stable competing Heusler phases of the 1221 structural and magnetic Mn-Ru-Ga cells investigated. The configurations investigated are limited to the primitive 4-atom Heusler cell (3-atom for half Heuslers) [19].

No.	4*a*	4*c*	4*b*	4*d*	ΔH (eV)	M (μ_B)	c/a	Volume (Å^3)
1	Mn	Ru	Ga	Ru	−1.11	2.18	1.0	56.33
2	Ga	Mn	Ga	Ru	−0.99	2.93	1.0	55.83
3	Mn	Mn	Ga	Ru	−0.97	0.07[a]	1.2	55.88
4	Mn	Mn	Ga	Ru	−0.52	4.66[b]	1.0	55.01
⋮	⋮	⋮	⋮	⋮	⋮	⋮	⋮	⋮
10	Ga	Mn	Ga		0.02	3.14	1.0	52.01
12	Ru	Mn	Ga		0.27	0.19	1.0	44.70
13	Ru	Mn	Ga	Ru	0.29	4.44	1.0	59.20
14		Mn	Ga	Ru	0.52	4.50	1.0	49.60
15	Mn	Mn	Ga		0.54	0.47	1.0	46.54
⋮	⋮	⋮	⋮	⋮	⋮	⋮	⋮	⋮

[a]Magnetization quenched by the tetragonal distortion.
[b]Ferromagnetic Mn_2RuGa phase.

For the Mn_2RuGa composition, we find that the lowest energy structure corresponds to Mn occupying the inequivalent 4*a*,4*c* sites, Ga the 4*b*, and Ru taking the remaining 4*d* site, consistent with literature [4,9]. Cubic Mn_2Ga was found to have a positive enthalpy of formation of 0.54 eV f.u.$^{-1}$, making the compound unstable with respect to decomposition into its elementary phases. The symmetry of the stable $D0_{22}$ structure was excluded from our calculations. However, the most energetically favorable Mn_2Ga structure in the $L2_1$ phase (No. 15) places Mn on the inequivalent 4*a* and 4*c* sites with Ga occupying the 4*b* site. The structure remains cubic and the magnetic state is ferrimagnetic, consistent with experimental characterizations presented by Kurt *et al.* [9] for thin films stabilized on a suitable substrate or a seed layer. We note that the formation of any half Heusler in the Mn, Ru, and Ga phase diagram is energetically unfavorable, so that we would not expect pure half Heuslers to be a significant constituent of the films.

We note that the energy of the system can be lowered by forming Mn-deficient $MnRu_2Ga$ or $MnGa_2Ru$ (No. 1 and No. 2 in Table I). Given that the difference in formation enthalpy of these phases with respect to Mn_2RuGa (No. 3 in Table I) is only 0.14 eV f.u.$^{-1}$, we expect that actual samples will not form distinct polycrystalline phases, but instead display significant site disorder, particularly on the 4*a* site, with a preference towards a lower Mn content. This was confirmed by laser-assisted inductively coupled mass spectroscopy (ICPMS) measurements of the Mn-to-Ga ratio for a series of samples with varying Ru concentration x. The ratio was observed to be in the 1.6–1.9 range, increasing with increasing film thickness [20].

In Fig. 2(a) we show scanning transmission electron microscopy (STEM) measurements of electron-transparent lamellae of Mn_2RuGa which indicate that there is little variation in either the in-plane or out-of-plane lattice constants throughout the film. The corresponding electron energy loss (EELS) spectra and line profiles are shown in Fig. 2(b). Alternating light and dark bands in dark-field images indicate slight compositional variations, especially in the layers closest to the surface. EELS measurements reveal that these bands correspond to layers of Mn enrichment and Ru depletion, suggesting a degree of phase segregation during growth, but not at the level of formation of half Heuslers. We also note that the Ru concentration x decreases by about 20% from the interface with the substrate through the thickness of the film; to a lesser extent, the Mn concentration increases across the same range.

In order to investigate the properties of low-Mn-content films we have performed supercell calculations where 1/3 of the Mn atoms at the 4*a* site are substituted with Ga. The Mn-Ga substitution simultaneously changes the lattice parameters, the magnetic properties, and the electronic structure of the system. We find that the ionic charges of Mn and Ga are +2 and +1, respectively. Hence a one-atom Mn-Ga substitution leaves the system with one unbound electron, thus creating electronic doping. Below we describe in detail the properties of such Mn-deficient compounds.

Lattice. Electronic doping provides an explanation for the variation of the lattice parameter with film thickness [21]. From the volume difference between the relaxed DFT structure and

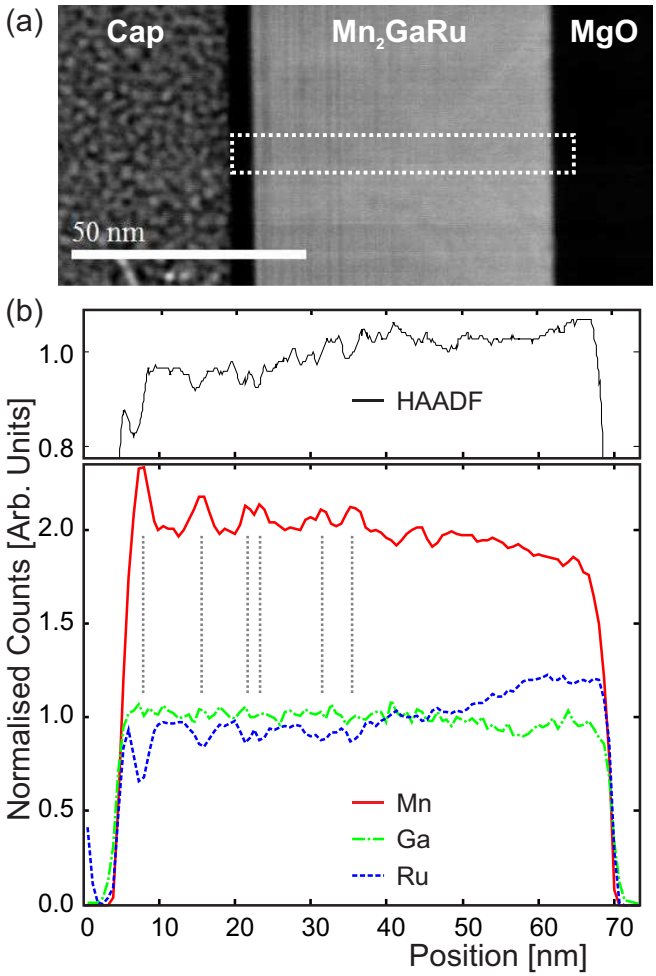

FIG. 2. Analytical electron microscopy analysis of the thin film ($x = 1$) composition. (a) High angle annular dark field (HAADF) image of a typical sample cross section, with the region where EELS data were acquired indicated by a white rectangle. In HAADF images, heavy elements appear brightest. (b) Elemental variations across the thin film stack, as measured by EELS. Data are normalized by setting the average composition to Mn_2GaRu. The dashed vertical lines indicate regions of Mn enrichment and Ru depletion, corresponding to darker features in the HAADF image.

the corresponding experimental one and by using the bulk modulus B_0, we estimate the experimental electronic doping. The bulk modulus is calculated for Mn_2Ru_xGa ($x = 0.0, 0.33, 0.50, 0.66$, and 1.0) compounds by fitting the Murnaghan equation of state [22,23]. By using a simple model

$$n_{\mathrm{el}} = \frac{B_0}{S_0}\left[\left(\frac{c}{a}\right)_{\mathrm{expt.}}\left(\frac{a_{\mathrm{expt.}}}{a_0}\right)^3 - 1\right], \qquad (1)$$

we can relate the experimentally observed lattice parameters to the electron doping level n_{el}. In Eq. (1) S_0 is the rate of change of the excess pressure with electron doping, while $a_{\mathrm{expt.}}$ and a_0 correspond to the experimental in-plane lattice constant and the relaxed theoretical lattice constant, respectively. This equation is easily derived under the assumption that the material is in mechanical equilibrium at the experimental lattice constant, due to the excess pressure provided by the Mn-Ga substitution,

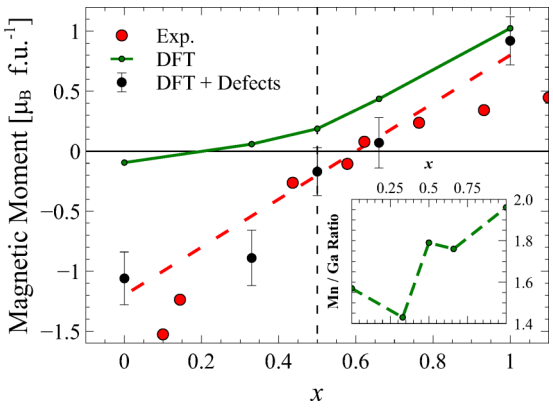

FIG. 3. Comparison of the magnetic moment predicted by DFT with the experimental results. The calculated magnetic moment for ideal MRG compounds is shown by the green line. Correction to the DFT magnetization due to the formation of Ga defects is shown by the black points. The corresponding estimate of the Mn/Ga ratio is shown in the inset. The dashed line equivalent to doping of 2 e/Ru is shown to guide the eye.

via the electron doping mechanism. Since we are comparing pressure differences, we ignore constant pressure terms. In order to stabilize the experimental lattice parameters, including the observed $c/a > 1$, we find electron doping in the range 0.1–0.5 e f.u.$^{-1}$, corresponding to a Mn/Ga ratio in the interval 1.4–2.0. The higher doping level occurs for the lower Ru concentrations, as shown in the inset of Fig. 3.

TEM imaging and spectroscopy clearly indicate that there are regions of high Mn content, and therefore regions of enhanced Ga content elsewhere in the sample. It is therefore reasonable to assume that films of different thicknesses will have a different electronic doping, which in turn alters the c-lattice parameter and does so uniformly throughout the sample.

Magnetism. A key feature of a CFHM is the magnetically compensated ground state. In agreement with Ref. [12], we find that the magnetization calculated for MRG compounds, as a function of the Ru doping, differs from the experimental one (see Fig. 3). The discrepancy is twofold: (I) The slope of the magnetization with x disagrees by a factor of 2, and (II) there is no compensation of the magnetization around $x = 0.5$. These discrepancies are resolved if we take into account the effect of the Mn-Ga substitution on the magnetic properties. Ga defects introduce, in addition to the electronic doping, a change in the net magnetic moment per unit cell, of $-2\mu_{\mathrm{B}}$ per Mn substituted by Ga, which allows us to express the expected moment M_{EXP} as

$$M_{\mathrm{EXP}}(x) = M_{\mathrm{DFT}}(x) - 2n_{\mathrm{el}}(x), \qquad (2)$$

where M_{DFT} is the theoretically calculated magnetic moment for a defect-free Mn_2Ru_xGa compound.

The corrections given by Eqs. (1) and (2) have been applied for each value of x, and the results are summarized in Fig. 3. Notably, the presence of defects improves significantly the agreement between the experimental and theoretical magnetic moments, with the exception of concentrations around $x = 1$. A neutron diffraction study by Hori *et al.* [4] has shown that the magnetization of stoichiometric Mn_2RuGa ($x = 1$)

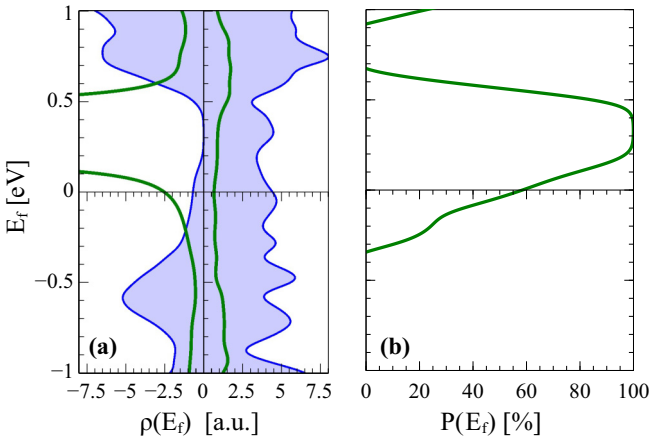

FIG. 4. (a) Spin resolved resistivity (green line) and the corresponding DOS (blue shadowed area) for electron-doped $Mn_2Ru_{0.5}Ga$. The doping was fixed at 0.4 electrons per formula. The data corresponding to the spin down channel are represented by negative values. (b) Calculated transport spin polarization.

is $\approx 1\mu_B$, in good agreement with our calculations. This leads us to the conclusion that in the $x = 1$ limit there may be a substantial content of the Ru_2MnGa phase, which is known to be antiferromagnetic [4].

Electronic structure. Finally, we discuss the effect of the electronic doping on the degree of transport spin polarization. In Fig. 4 we show the DOS and corresponding Boltzmann resistivity for Mn_2RuGa with $n_{el} = 0.4$ extra electrons per formula unit, corresponding to a Mn/Ga ratio of 1.6 as observed by ICPMS. The additional doping results in a transport spin polarization of ≈60%, which is twice as large as the one calculated for the original Mn_2Ru_xGa compound. At a doping level of $n_{el} = 1.0$ the transport spin polarization becomes 100%. It is important to note that the calculations presented here do not take into account the effect of the disorder due to the Mn-Ga substitution on the transport properties. The stoichiometry has been shown to vary across the film as shown in Fig. 2, and we would therefore expect a variation of the electronic structure which will in turn reduce the spin gap [12]. However, the robustness of the experimentally observed spin polarization can only be rationalized if a wide enough disorder-induced transport spin gap exists at the Fermi level. Disorder introduces a smearing to the band picture, reducing conductivity in both spin channels through Anderson localization [24]. Localization of the states originates at the band edge, leaving the center of the band delocalized [25]. In MRG the Fermi level lies at the edge of the majority spin band, whereas for the minority it is at the band center. We would therefore expect that localization to affect the conductivity of the majority spin channel more than the minority, resulting in an increased transport spin polarization. Chadov *et al.* have demonstrated that this mechanism is applicable in the $Mn_{3-x}Co_xGa$ system [26].

Ideal half metallicity exists only in the zero-temperature limit, and in the absence of spin-orbit interaction. Compensation for practical materials under ambient conditions occurs at a specific temperature, which can be tuned by composition and strain, while maintaining the Fermi level in the spin gap. This can be achieved because, unlike an antiferromagnet, the two magnetic sublattices have different temperature dependences [7,11].

In conclusion, a sustained dialogue between experimental measurements and theoretical calculations has demonstrated that Mn_2Ru_xGa can form a true CFHM. As a consequence, we expect that it may become a cornerstone for future spintronics technology. By means of high-throughput calculations, we have shown that there are several competing phases in the Mn-Ru-Ga system, and that due to their small energy differences they exhibit a strong tendency towards site disorder, and a preference for reduced Mn content. This has all been confirmed by our experimental characterization of MRG thin films. Furthermore, the low Mn content provides an electronic doping mechanism, pushing the system towards half metallicity and improving the agreement between experiment and theory regarding the structural and magnetic properties of the system. Based on our calculations, complete transport spin polarization can be achieved.

We have shown that the chemical composition, c/a ratio, tendency to site disorder, and cell volume are all correlated. To achieve transport half metallicity and zero net moment, a reduced Mn to Ga ratio of ≈1.4 is required, as well as a Ru concentration of ≈0.7. Fine tuning of the position of the Fermi level in the spin gap can then be achieved through varying the c/a ratio, which we have shown can be done by varying the film thickness.

The authors would like to thank Cora McKenna for the ICPMS mesaurements, and H. Kurt for fruitful discussions. Computational resources have been provided by the Trinity Center for High Performance Computing (TCHPC) and by the Irish Centre for High-End Computing (ICHEC). The authors acknowledge financial support from the FP7 project "ROMEO" (Grant No. 309729), Science Foundation Ireland through "AMBER," and from Grant No. 13/ERC/12561.

[1] H. van Leuken and R. A. de Groot, Phys. Rev. Lett **74**, 1171 (1995).
[2] M. Hakimi, M. Venkatesan, K. Rode, K. Ackland, and J. M. D. Coey, J. Appl. Phys. **113**, 17B101 (2013).
[3] L. Yang, B. Liu, F. Meng, H. Liu, H. Luo, E. Liu, W. Wang, and G. Wu, J. Magn. Magn. Mater. **379**, 1 (2015).
[4] T. Hori, M. Akimitsu, H. Miki, K. Ohoyoama, and Y. Yamaguchi, Appl. Phys. A: Mater. Sci. Process. **74**, s737 (2002).
[5] S. Wurmehl, H. C. Kandpal, G. H. Fecher, and C. Felser, J. Phys.: Condens. Matter **18**, 6171 (2006).
[6] I. Galanakis, P. Mavropoulos, and P. H. Dederichs, J. Phys. D: Appl. Phys. **39**, 765 (2006).
[7] E. Şaşıoğlu, Phys. Rev. B **79**, 100406 (2009).
[8] X. Hu, Adv. Mater. **24**, 294 (2012).
[9] H. Kurt, K. Rode, P. Stamenov, M. Venkatesan, Y.-C. Lau, E. Fonda, and J. M. D. Coey, Phys. Rev. Lett. **112**, 027201 (2014).

[10] N. Thiyagarajah, Y.-C. Lau, D. Betto, K. Borisov, J. M. D. Coey, P. Stamenov, and K. Rode, Appl. Phys. Lett. **106**, 122402 (2015).
[11] D. Betto, N. Thiyagarajah, Y.-C. Lau, C. Piamonteze, M.-A. Arrio, P. Stamenov, J. M. D. Coey, and K. Rode, Phys. Rev. B **91**, 094410 (2015).
[12] I. Galanakis, K. Özdoğan, E. Şaşioğlu, and S. Blügel, J. Appl. Phys. **116**, 033903 (2014).
[13] I. Galanakis, P. H. Dederichs, and N. Papanikolaou, Phys. Rev. B **66**, 134428 (2002).
[14] See Supplemental Material at http://link.aps.org/supplemental/10.1103/PhysRevB.93.140202 for DFT calculation details.
[15] T. Timusk and B. Statt, Rep. Prog. Phys. **62**, 61 (1999).
[16] See Supplemental Material at http://link.aps.org/supplemental/10.1103/PhysRevB.93.140202 for c/a variation with film thickness.
[17] G. Y. Sun, J. Kürti, P. Rajczy, M. Kertesz, J. Hafner, and G. Kresse, J. Mol. Struct.: THEOCHEM **624**, 37 (2003).
[18] J. P. Perdew, K. Burke, and M. Ernzerhof, Phys. Rev. Lett. **78**, 1396 (1997).
[19] http://www.materials-mine.com
[20] See Supplemental Material at http://link.aps.org/supplemental/10.1103/PhysRevB.93.140202 for mass spectroscopy measurements.
[21] See Supplemental Material at http://link.aps.org/supplemental/10.1103/PhysRevB.93.140202 for the doping model.
[22] C. L. Fu and K. M. Ho, Phys. Rev. B **28**, 5480 (1983).
[23] F. D. Murnaghan, Proc. Natl. Acad. Sci. USA **30**, 244 (1944).
[24] P. W. Anderson, Phys. Rev. **109**, 1492 (1958).
[25] B. Kramer and A. MacKinnon, Rep. Prog. Phys. **56**, 1469 (1993).
[26] S. Chadov, J. Kiss, and C. Felser, Adv. Funct. Mater. **23**, 832 (2013).